Title:

A high-throughput multiplex array for antigen-specific serology with automated analysis.

Rosenberg, A.F.[1], Killian, J.T. Jr.[1], Green, T.J.[1], Akther, J.[3], Hossain, M.E.[1], Qiu, S Randall, T.D.[2], Lund, F.E.[1], and King, R.G.[1]

Affiliations:

[1]Department of Microbiology, University of Alabama at Birmingham (UAB), Birmingham, AL 35294, USA

[3]Department of Medicine, Division of Clinical Immunology and Rheumatology, UAB, Birmingham, AL 35294, USA

*Corresponding author: rgking@uab.edu

Abstract.

High-throughput customizable CBA automated script-based analysis.

The utility of high-throughput systems to evaluate antigen-specific Ab has been highlighted by the SARS-CoV-2 pandemic. Pathogen specific antibody levels are often used to assess protection following vaccination and, in the case of novel pathogens, an indication of prior exposure. Several platforms exist to visualize antigen-specific Ab, however most are not quantitative and difficult to scale for population levels studies. Additionally, the sensitivity across platforms differs making direct comparisons between studies difficult. Cytometric Bead Arrays are an attractive platform for antigen-specific Ab measurements as they allow antibodies reactive against several antigens and of several isotypes to be performed simultaneously. Additionally, cytometric arrays exhibit a high sensitivity and can be designed to provide quantitative measurements. Using commercially available particles, a biotin-Streptavidin loading strategy, and the inclusion of indirect standards, we describe here a flexible system that can be modified to include a variety of antigens. We generated two arrays, one focused on β-Coronavirus antigens and one focused on Influenza. To support the high throughput capacity of this system, we developed a suit of automated tools to process raw data into antigen-reactive IgM, IgA, and IgG. We describe quality control requirements, assay performance, and normalizations to accurately quantitate antigen specific Ig.

1. Introduction

Serum antibody (Ab) levels targeting pathogens have been used to predict protection, determine exposure history, and provide a measure of efficacy of vaccination. The ongoing COVID pandemic has highlighted the need for rapid and accurate quantification of antigen-specific Abs in human serum or fluid samples. Early in 2020, the human immune response to SARS-CoV-2 was uncharacterized and considerable effort was devoted to determining how individuals responded to infection, and whether there were correlates of Ab responses to disease outcomes. Even following the approval of multiple SARS-CoV-2 vaccines, it was unclear what serological features of the humoral immunity afforded protection from infection or re-infection. Unfortunately, the evolution of the Sars-2-CoV-2 pandemic over the last couple years have illuminated the shifting landscape of variants and the uneven protection afforded by the original vaccination formulations [1, 2]. Despite numerous published studies, some involving large-cohorts, addressing the magnitude and longevity of SARS-CoV-2 humeral immunity, there remains a need for inexpensive, high-throughput methodologies to evaluate Ab responses following or infection or vaccination [3, 4]. Additionally, it is now clear that not all Abs directed toward the Sars-2-CoV spike protein (C SP) are protective, necessitating the visualization of C SP sub-domain reactivity as well as the distribution of Abs across isotypes and toward new emerging variants. Although several platforms have been described to evaluate SARS-CoV-2-reactive Abs including [5-12], few of these methodologies are quantitative, making direct comparisons across platforms or the cohorts targeted in these studies difficult, thereby hampering our ability to define levels of Ab reactive with C SP or subdomains that correlate with protection. Such analyses are becoming increasingly important as SARS-CoV-2 variants resistant to prior vaccine responses continue to emerge [2]. Although the covid pandemic has increased the awareness of the utility of platforms to evaluate antigen specific Ab, such platforms are important for a host of other pathogens including seasonal influenza (INF) virus. To address this need, we developed a highly customizable cytometric bead array platform to quantitate specific Abs against several pathogen associated antigens of IgG, IgM, and IgA subclasses. Coupled with a

automated MATLAB analysis pipeline, this system allows for the high-throughput quantification of Abs reactive to a wide variety of antigens.

Cytometric bead arrays have been widely employed to determine the concentration of diverse analytes from biological samples including Abs [cite CBA review]. They offer several advantages over other traditional approaches including the ability to multiplex ligands, enhanced sensitivity compared to traditional ELISA assays, and a broad dynamic range[10, 13]. Because of these properties, CBAs are an attractive platform to quantitate Abs reactive to many antigens simultaneously in a high-throughput format.

Here we describe the generation of a highly multiplexed CBA system to evaluate antigen specific Ab responses and describe its use targeting two pathogens. One array consists of 12 antigens derived from B-CoV virus spike ectodomains (SP) and nucleocapsid proteins (NP). The second incorporates 14 INF hemagglutinins (HA) in addition to influenza NP and non-structural protein 1 (NS1). To support this platform, we developed a post-acquisition, MATLAB-based analytic pipeline to streamline data analysis and enable high-throughput use. In addition, we have evaluated the performance of the array using panels of monoclonal and polyclonal human Abs providing antigen specific and generalizable corrections allowing for the accurate quantification of serum Ab of the IgM, IgA, and IgG subclasses toward each of the array constituents. Although the configuration of the arrays described here are focused on B-CoV and INF derived antigens, the platform is flexible and utilizes indirect standards which allow for the Ab reactive to essentially any protein antigen to be quantitated.

2. Material and methods

2.1 *Array generation*.

Cytometric array described here was constructed using spherotech 4um and 5um Carboxy Blue Particle Array Kits (Spherotech CPAK-4067-8K and CPAK-5067-10K respectively). Antigens were loaded by first conjugating Streptavidin (SA) to via amide using commonly employed 1-Ethyl-3-(3-dimethylaminopropyl)carbodiimide (EDC) chemistry. Streptavidin (SA) (Southernbiotech 7105-01) was buffered exchanged using PD-10 columns (Cytiva 17085101) into PBS and diluted to 2mg/mL. For conjugation,

99 10e8 shperotech particles were isolated by centrifugation at 10,000Xg for 3 min. After
100 carefully removing the supernatant, the bead pellet was resuspended in 0.5 mLs of SA in
101 PBS. Following complete resuspension by pipetting, 0.5 mLs of 6mM EDC dissolved in
102 0.05M MES buffer PH 5.0 was added, and the reaction mixture was rotated at room
103 temperature overnight. After the conjugation reaction was complete, 0.1 mL of 1M tris PH
104 8.0 was added to quench the reaction. Following a 1 hr incubation, the beads were
105 harvested by centrifugation as described above and washed twice in 1mL of PBS.
106 Following the final wash, beads were resuspended in $1e10^8$ particles/mL of PBS with
107 0.25%NaN3 and stored at 4deg.

108 Following SA conjugation, quality control experiments were performed to
109 determine the degree and uniformity (when multiple particle sizes and/or peak identities
110 are used) of labeling by staining the SA-conjugated particles with fluorescently- labeled-
111 biotinylated hemagglutinin (PR8). Individual array constituents were mixed and diluted to
112 1e6 of each particle/mL. 40ul of serial dilutions of PR8 were prepared in a 96 well U
113 bottom plate (Corning 3797) ranging from 1ug/mL to 2ng/mL. 5ul of the bead suspension
114 was added, mixed by pipetting, and incubated for 15 min at RT. 200ul of PBS was then
115 added and the plate was centrifuged at 3000Xg for 5min. The beads were resuspended
116 in 80uL of PBS. Samples were then analyzed by flow cytometry.

117 Following SA coupling and quality control procedures described above, biotinylated
118 recombinant array antigens were passively absorbed onto the individual particles. For
119 antigens described here (table 1), a single biotin site was added enzymatically onto a
120 carboxy terminal AVI tag. SA conjugated particles were harvested by centrifugation as
121 described above and resuspended in 1mg/mL of the recombinant proteins in 1%BSA in
122 PBS. Antigen loading was carried out by rotating overnight at 4deg. Following absorption,
123 the beads were harvested by centrifugation as described, and washed twice with 1% BSA
124 in PBS. Finally, the antigen coated beads were resuspended at 1e8 particles/mL 1% BSA
125 in PBS, 0.25% NaN3 and stored at 4deg until use.

126

127 *2.2 Recombinant antigens.*

128 *Production of pre-fusion recombinant Spike (S) proteins.* Ectodomain S pre-fusion trimers
129 (SARS-CoV-2 $S_{14\text{-}1211}$) were produced by co-transfecting S-AviTag and S-6X-HisTag

130 constructs into FreeStyle 293-F Cells at a 1:2 ratio. Transfected cells were cultured in
131 FreeStyle 293 Medium for 3 days and recombinant S trimers purified from culture
132 supernatant by FPLC using Nickel-affinity chromatography. Purified proteins were
133 biotinylated by BirA enzyme in vitro.

134 *Production of S subdomains*. NTD (SARS-CoV-2 S_{14-305}) and RBD (SARS-CoV-2 S_{319-}
135 $_{541}$) monomers with a C-terminal dual AviTag/6X-HisTag sequence were produced by co-
136 transfecting single constructs into FreeStyle 293-F Cells. Following a 3-day expression,
137 subdomains were purified from culture supernatant by FPLC using nickel-affinity
138 chromatography and biotinylated by addition of BirA.

139 *Production of CoV nucleocapsid protein (N).* Recombinant N containing the full-length N
140 and tandem AviTag/6X-HisTag sequence were produced by co-transforming Rosetta
141 cells with the N expression plasmid and an inducible BirA expression plasmid. Cells were
142 grown in the presence of chloramphenicol, ampicillin, and streptomycin, induced with
143 IPTG and supplemented with biotin. Biotinylated N protein was purified by FPLC using a
144 nickel-affinity column and subsequent size exclusion chromatography.

145 *Recombinant influenza HA protein production*. The nucleic acid sequence corresponding
146 to amino acids 18-524 of influenza HA ectodomains purchased and synthetic genes
147 (GeneArt, Regensburg, Germany) from influenza virus strains listed in table 1 as
148 previously described [14], synthetic constructs were cloned into the pCXpoly(+) vector
149 modified with a human CD5 leader sequence and a GCN4 isoleucine zipper trimerization
150 domain (GeneArt) followed by either a 6XHIS tag (HA-6XHIS construct) or an AviTag
151 (HA-AviTag construct). The HA–6XHIS and HA–AviTag constructs for each HA were co–
152 transfected using 293Fectin Transfection Reagent into FreeStyle™ 293–F Cells
153 (ThermoFisher Scientific) at a 2:1 ratio. Transfected cells were cultured in FreeStyle 293
154 Expression Medium for 3 days. The supernatant was then cleared by centrifugation.
155 Recombinant HA molecules were purified from these culture supernatants by FPLC using
156 a HisTrap HP Column (GE Healthcare) and eluted with 250 mM imidazole.

157

158 *Production of influenza NP and NS1 proteins.*

159 The coding sequence of NP from PR8 was synthesized in frame with the coding sequence
160 for a 15–amino acid biotinylation consensus site [15] on the 3′ end (GeneArt). The
161 modified NP sequence was cloned in frame to the 6X His tag in the pTRC–His2c
162 expression vector (Invitrogen). NP protein was expressed in E. coli strain CVB101
163 (Avidity), purified by FPLC using a HisTrap HP Column (GE Healthcare) and eluted with
164 a 50–250 mM gradient of imidazole. Coding sequence for the influenza virus A/PR8/34
165 NS1 gene (amino acids 3–230, Accession Number: AAA43536) was chemically
166 synthesized (GeneArt) in frame with a 3' addition of the coding sequence for the BirA
167 enzymatic biotinylation consensus site136 and the 6X-His purification tag. Two mutations,
168 R38A and K41A, demonstrated to prevent aggregation of NS1 at high concentrations137,
169 were introduced into the NS1 gene by site-directed mutagenesis. The recombinant NS1
170 gene was cloned into the pTRC–His2c expression vector (Invitrogen) and expressed in
171 the BirA-enzyme containing E. coli strain CVB101 (Avidity) Biotinylated recombinant NS1
172 was purified by FPLC using a HisTrap HP Column (GE Healthcare), eluted with a 50–250
173 mM imidazole gradient, buffer exchanged and concentrated.

174

175 *Antibodies and standards.*

176 Detection of IG fluorescent goat polyclonal anti-IG F(ab')2 secondaries, Southern Biotech
177 (IgM cat 2022-02, IgG cat# 2062-09, IgA cat# 2052-09) Isotype standards were generated
178 by performing the array on mixtures of IG capture beads with 0.75x serial dilutions of
179 purified human Abs southern biotech (IgG cat# 0150-01, IgM Cat# 0158L-01, IgA
180 cat#0155L-01) in ranging from 1ug/mL to 1.3 ng/mL. Anti-SARS Abs JTK137_H22 and
181 JTK137_K6 were generated from the C SP binding B cells derived from a vaccinated
182 donor. The C SP reactive Ab CR3022 was acquired from IDT Biologika. C SP reactive ab
183 AHA001 was purchased from Sanyou Bio. HA-reactive Abs (P52d7_K12, P52d7_I1, and
184 P52d7_D20) were generated from HA-binding B cells from a vaccinated donor [16].
185 Polyclonal anti-C SP reactive Ab was purified from the serum of a vaccinated donor using
186 affinity chromatography. Briefly, 0.5 mg of purified C SP trimers generated as described
187 was conjugated to cyanogen bromide activated Sepharose (GE) following manufactures
188 protocol. 10mLs of serum was diluted into 40mLs of PBS filtered using a 0.45um syringe

filter (Corning 431220). C SP conjugated Sepharose was added and rotated overnight at 4deg. The resin was collected by centrifugation at 2000g for 10min and washed twice with 50 mL of cold PBS. After the final wash, the resin was loaded into a disposal micro column (Pierce 89868) and eluted with 5 fractions of 200ul of 0.1M glycine pH 2.8 into 25ul of 1M tris pH 9.0. Eluted fractions were pooled and concentrated by centrifugation through an 30K centrifugal filter (Millipore Sigma UFC500324). Following concentration, the samples was buffer exchanged into PBS using a 0.5mL Zeba column (Fisher scientific PI87767) and quantitated.

2.3 Assay protocol

Serum samples were diluted into PBS (1/7150 for IgG detection, or 1/500 for IgM and IgA detection) and arrayed in 96 well u-bottom plates. A 5µl suspension containing 5x1e5 of each antigen coated microparticles was added to the samples. In the case of Ig standards, anti-IgM, anti-IgA, and anti-IgG beads were added to 50ul of the serial dilutions of standard Abs. The suspensions were mixed by pipetting and incubated for 15 mins at room temperature. The beads were washed by the addition of 200µl of PBS and centrifugation at 3000g for 5min at room temperature. The CBA particles were resuspended in a secondary staining solution consisting of the appropriate anti-Ig secondary diluted 1/400 in 1%BSA in PBS. The suspension was incubated for 15 min in the dark at room temperature. The beads were washed by the addition of 200 µl of PBS and pelleted by centrifugation at 3000g for 5 min at room temperature. The particles were resuspended in 80µl of PBS and directly analyzed on a BD Cytoflex flow cytometer in plate mode at sample rate of 100ul per minute. Sample collection was stopped following the acquisition of 75 µL. Following acquisition, the resulting FCS files were processed using the software described below.

2.4 Automated analysis and software

We developed custom software to automatically process FCS files to rapidly quantify the Ab reactivities of serum samples. This software was developed in Matlab (The Mathworks, Inc. Natick MA, USA) version R2020a on MacOS. It requires the Statistics and Machine Learning Toolbox, the Curve Fitting Toolbox and the Signal Processing

220 Toolbox. Additionally, code from Matlab Central (www.mathworks.com/matlabcentral/)
221 public code repository was incorporated into this program [17-20]. This software is
222 available on GitHub [link here].
223
224 2.5 *Human serum samples.*
225 Human serum samples were collected as part of the UAB Cooperative Centers for
226 Human Immunology program from organ donors. Peripheral blood from human subjects
227 was drawn into K2-EDTA tubes (BD Bioscience). Plasma were isolated by density
228 gradient centrifugation over Lymphocyte Separation Medium (CellGro), aliquoted, and
229 stored in LN2. Cryopreserved samples were thawed at room temperature and diluted
230 1/100 in PBS in a 96 well U bottom plate to generate a 'master plate' stored at -20 deg.
231 Final dilutions were generated in assay plates as needed. For assay optimization and
232 dilution determination serum was derived from consented participants under the UAB
233 Institutional Review Board approved the study protocol (IRB-300005127).
234
235 **3. Results and discussion**
236 *3.1 Generation of the B-COV and INF arrays.*
237 To simultaneously interrogate Ab reactivity to multiple viral protein antigens, we
238 adopted a commercially available cytometric array platform by spherotech and an indirect
239 conjugation methodology. Streptavidin is conjugated to carboxy modified microparticles
240 using commonly employed EDC chemistry to allow for the passive absorption of
241 biotinylated antigen onto each individual bead. Our strategy is to maximize SA
242 conjugation such that the binding capacity of each bead is high and uniform, followed by
243 the absorption of antigens at saturating concentrations. The uniformity of SA loading is
244 evaluated by staining bead preparations with a recombinant influenza hemagglutinin
245 (PR8) trimer, containing a single N-terminal biotin site, fluorescently labeled with Alexa
246 488. The intensity of labeling relates to the absorption of the fluorescent trimer and is
247 typically uniform across the array (FIG 1). The particles sizes exhibit different maximum
248 intensities, in part due to the difference of surface area between the 4um and 5um
249 particles (Fig 1c). SA loading is uniform within the constituents of each particle size,

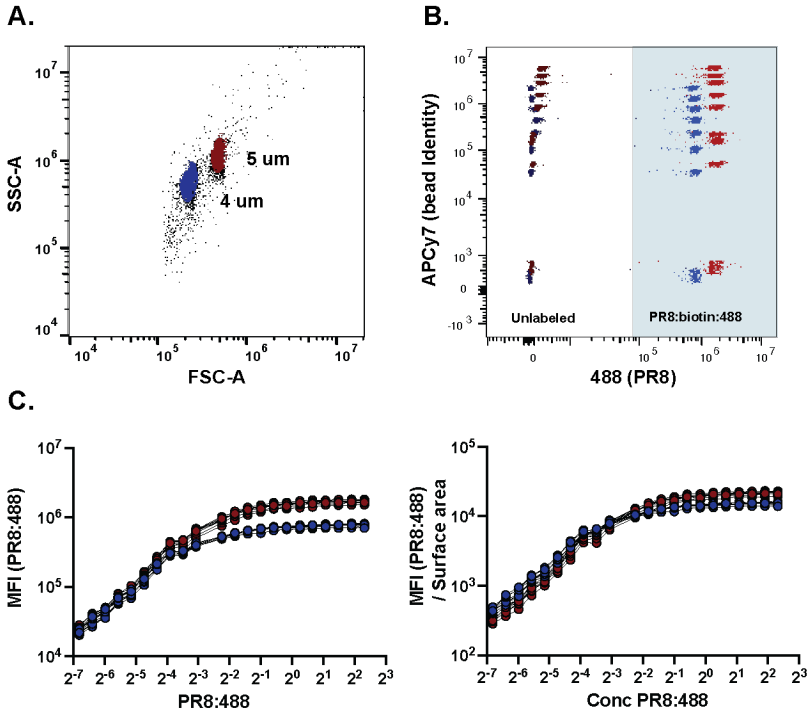

Figure 1. Array generation and loading controls. A. Forward and side scatter histograms for differentiating the indicated size particle. **B.** Flow cytometric histogram of the array constituents before (left, unshaded) and following incubation with biotinylated / alexa488 influenza hemagglutinin PR8 (right, shaded). **C.** Mean fluorescent intensity of each array constituent (left) and corrected (right) by relative surface area when stained with the indicated concentration of PR8:biotin:488.

however, with a coefficient of variation of 5.39% and 5.34% for all 5um and 4um beads respectively. The array exhibits a highly uniform decay of signal as a function of analyte concentration, suggesting both that the binding capacity of each bead is uniform and that the binding is highly dependent on analyte concentration.

To determine the binding capacity of the SA conjugated beads, we adopted two independent approaches. First, we incubated the SA conjugated particles with an excess of a known but variable amount of biotinylated influenza hemagglutinin trimers,

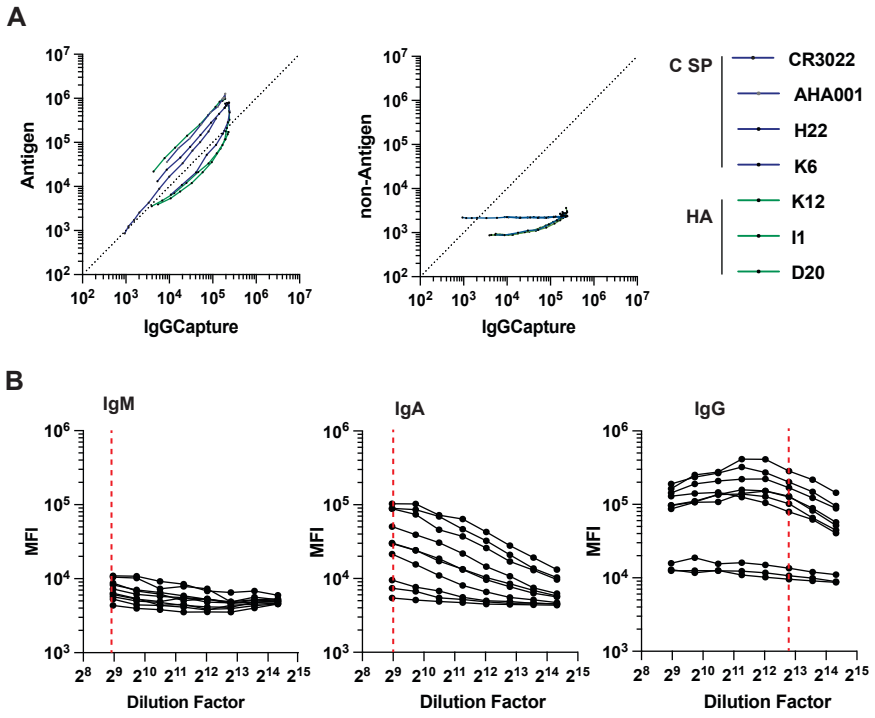

Figure 2. Dilution curves of antigen specific antibodies. **A.** Plots of the MFI of antigen-coated and anti-IgG CBA beads stained with serial dilutions of the indicated CS SP (green lines) or CA09 (blue lines) reactive mAbs. **B**. MFI of CS SP Beads stained with serial dilutions of human serum from COVID convalescent patients visualized with secondaries reactive to the indicated human Ig isotype.

and measured the protein absorbed from these suspensions. For the two independent lots of SA-conjugated beads tested, an average equivalent of 220ug per $1X10^8$ particles was absorbed. Next, we incubated the SA beads with decreasing concentrations of fluorescently labeled PR8 as described above, as assayed the mean fluorescence intensity. The point of inflection at which concentration the beads appear to be subsaturated equates to the same value, 200ug of PR8 per 1X1e8 beads, thus we estimate the typical biotin binding capacity of SA beads to be 0.1 picomole per particle.

3.2 Array validation and characterization:

To generate a B-CoV focus array, we absorbed SARS-CoV-1, and SARS-CoV-2 full length, pre-fusion stabilized trimers as well as monomeric RBD subunits of these proteins

271 **Table 1.**

Influenza			
Peak #	**Antigen**	**Antigen description**	**Protein Accession #**
5uM-1	PR8	Influenza HA (H1)	MH785011.1
5uM-2	CA09	Influenza HA (H1)	NC_026433.1
5uM-3	Hawaii2019	Influenza HA (H1)	MN976432.1
5uM-4	MICH15	Influenza HA (H1)	MK622940.1
5uM-5	Brisbane	Influenza HA (H1)	MN569031.1
5uM-6	X31	Influenza HA (H3)	DQ874876.1
5uM-7	TX50	Influenza HA (H3)	KC892952.1
5uM-8	SW13	Influenza HA (H3)	EPI543739
5uM-9	SING2016	Influenza HA (H3)	EPI2053182
4um-2	HK2014	Influenza HA (H3)	NA
4um-3	NETH1999	Influenza HA (H2)	CY122252.1
4um-4	VN2004	Influenza HA (H5)	HM006759.1
4um-5	CAN04	Influenza HA (H7)	CY015013.1
4um-6	HongKong2013	Influenza HA (H9)	NA
4um-7	INF NP	Influenza Nucleocapsid protein	NCAP_I34A1
4um-8	INF NS1	Influenza Non-structural protein	AAA43536
B-CoV			
4um-2	S NP	Sars-CoV-1 Nucleocapisid Protien	AAP13445.1
4um-3	M NP	MERS Nucleocapisid Protien	P_009047211.1
4um-4	O NP	OC43 Nucleocapisid Protien	KR055606.1
4um-5	H NP	HKU1 Nucleocapisid Protien	Q5MQC6.1
4um-6	C NP	Sars-CoV-2 Nucleocapisid Protien	QHD43423
5uM-1	S SP	Sars-CoV-1 Spike ectodomain	AAX16192.1
5uM-2	S RBD	Sars-CoV-1 Receptor binding domain	AAX16192.1
5uM-3	CS SP	Sars-CoV-2 Spike ectodomain	QHD43416.1
5uM-4	CS RBD	Sars-CoV-2 Receptor binding domain	QHD43416.1
5uM-5	CS NTD	Sars-CoV-2 N-Terminal domain	QHD43416.1
5uM-6	M SP	MERS Spike ectodomain	AKI29255.1
5uM-7	O SP	OC43 Spike ectodomain	AAT84362.1
5uM-8	H SP	HKU1 Spike ectodomain	Q5MQD0.1
5uM-9	CA09	Influenza HA (H1)	NC_026433.1

272

273 **Table 1. List of antigens used to generate the Inf and CoV antigen Arrays.**
274 The size and peak number of each array element is listed, with the biotinylated
275 recombinant protein loaded to generate the two arrays. The protein accession numbers
276 are provided.

277

278

279 and the NTD of SARS-CoV-2 onto constituents of the array. Additionally, we chose two
280 related B-CoV spike proteins derived from HKU1 and OC43, as well as the nucleocapsid
281 proteins from all of these viruses, and finally, INF HA (CA09) to serve as an unrelated
282 positive control. The distribution of these molecules within the array is listed in Table 1.

283 For the antigens for which mAbs were available, antigen loading was validated by specific
284 mAb staining. When the mAbs I1 and CR3022, reactive with CA09 and C SP respectively,
285 were subjected to the assay, the MFI derived from antigen coated beads were highly
286 correlated with IgG capture beads conjugated with anti-human IgG, and nearly identical
287 for each mAb-antigen at a range of 1ug/mL to 1ng/mL. In contrast, the staining of I1 and
288 CR3022 to non-cognate antigen coated beads was minimal for both mAbs (Fig 2a). These
289 data demonstrate the effective range and sensitivity of the assay, which is linear for nearly
290 three orders of magnitude and can reliably detect Abs present at 10ng/mL in this
291 configuration.
292
293 *3.3 Assay functional range and dilution factor determination*
294 Constituents of the B-CoV array, like most cytometric bead arrays, exhibits significant
295 prozone effect at high Ab concentrations (Fig 2b) . This is especially true when polyclonal
296 sera are analyzed. Despite the large dynamic range, it is important to choose dilutions at
297 which the resulting MFI can be accurately extrapolated to concentration. To determine
298 the Ab concentration at which the prozone effect is observed and to identify a dilution
299 range allowing for the determination of antigen reactive IgG, IgM, and IgA. We analyzed
300 ten convalescent serum samples a dilution factor between 1/500 and 1/20517. As can be
301 seen in fig 3, the detection of IgG yielded significantly different maximum intensities and
302 dilution curves then IgA and IgM. For samples that contained detectable anti-C SP IgG,
303 the prozone effect was apparent at dilutions up to 1/7000 after which the signal decayed
304 as a function of Ab concentration. IgM and IgA signals, although detectable at 1/7000 in
305 some samples, never reached a concentration that exhibited prozone effects. This
306 difference is likely due to both the relative concentrations of these Ig subclasses and
307 differences in the signal intensity derived from the isotype specific secondaries. Using this
308 experiment as a guide, we selected a 1/7100 dilution for IgG 1/500 for IgM/IgA in
309 subsequent experiments. Depending on the Ab levels within a cohort and the antigen of
310 interest, these parameters require empirical identification.
311
312 *3.4 Antibody standards and quantification:*

313 Although the data described above suggested that the CBA would provide sensitive
314 quantitative assessment of the presence of specific Ab, we sought to refine the assay to
315 accurately measure antigen specific Ab present in biological specimens. We first
316 attempted to utilize monoclonal Abs of defined reactivity toward C SP and HA to generate
317 antigen-specific standards. Although this is a traditional approach, the relationship
318 between Ab concentration and MFI resulting from monoclonal Abs is dependent several
319 factors, including the distribution of Ab isotype, which are unequally recognized by pan
320 IgG secondaries, the affinity of the Ab, and the valency of Ab-antigen interactions.
321 Because the derived MFI results from the association of the fluorescently labeled
322 secondary Abs with the beads is independent of the nature of the antigen, we passively
323 absorbed biotinylated anti-Ig secondaries onto the matched SA conjugated beads used
324 to generate the antigen array. To determine the accuracy of these assessments, we
325 compared the MFI of antigen coated and standard beads following staining with mAbs
326 reactive against either C SP or HA visualized with fluorescently conjugated anti-IgG
327 secondaries. As seen in figure 2, the signals derived from both the antigen coated and
328 Ig capture conjugated bead were highly similar across the dilution range, although the
329 ratio differed for each monoclonal. This likely reflects differences in the affinity of these
330 mABs, as has been described for HA reactive Abs [16]. These data suggest that
331 biotinylated anti-isotype capture Abs serve as an accurate surrogate for the
332 quantification of bead-bound antigen and, assuming the antigen density was equivalent,
333 as an indirect standard for the Ab quantification. To control for differences in the binding
334 capacity between different particle sizes, and minor deviations between the individual
335 array components, we generated a panel of ig-capture beads, distributing the IgM, IgA,
336 and IgG capture Abs on every third bead peak across all the individual constituents of
337 the array. Purified IgM, IgA, or IgG was serially diluted from 1ug/mL to ~1ng/mL to
338 correlate the MFI of the capture beads to the quantity of the standard, and these curves
339 were then used to extrapolate the Ab isotype bound to the antigen specific beads
340 providing an accurate quantification (Fig S2).
341
342 *3.5 Automated Analytic Workflow*

Although the array data is collected using a traditional flow cytometer and can be analyzed by any number of flow cytometric software packages, the inclusion of multiple standard curves and the large number of individual flow files make manual data processing laborious. Additionally, although antigen specific Ig concentrations are derived values determined following the export of MFI values corresponding to each bead peak and the application of a curve derived from the standards, the quality of each sample must be determined individually with traditional flow analysis software prior to data export rendering this method labor intensive and error prone. To circumvent these problems and perform automated sample quality assessments and batch processing, we developed software pipeline that automatically processes raw data files from the cytometer to construct sample-by-feature tables of Ab concentrations. This software, written in Matlab (The Mathworks, Inc., Natick MA, USA), processes individual raw FCS files to identify events associated with beads, find peaks, summarize data, and enables a batch mode which can process many files at once including standard controls useful for back-calculating concentration units from mean fluorescence intensity (MFI) data. The overall workflow is shown in Figure 3. The command line program requires four arguments: a directory containing all the FCS files, a sample manifest containing metadata for each of the corresponding FCS files (including the flow cytometry channel mappings for the bead channel and the secondary isotype channel), a configuration file describing the association of bead peak order with protein for the specific assay, and a configuration file containing parameters for peak identification. The output is a Matlab structure array where each element contains a table of isotype reactivity for each feature in the assay as well as other program settings for complete analytical provenance to support reproducibility. This structure array, in turn is used for an analysis quality assessment program to visually summarize the consistency of the bead gates for each bead size as

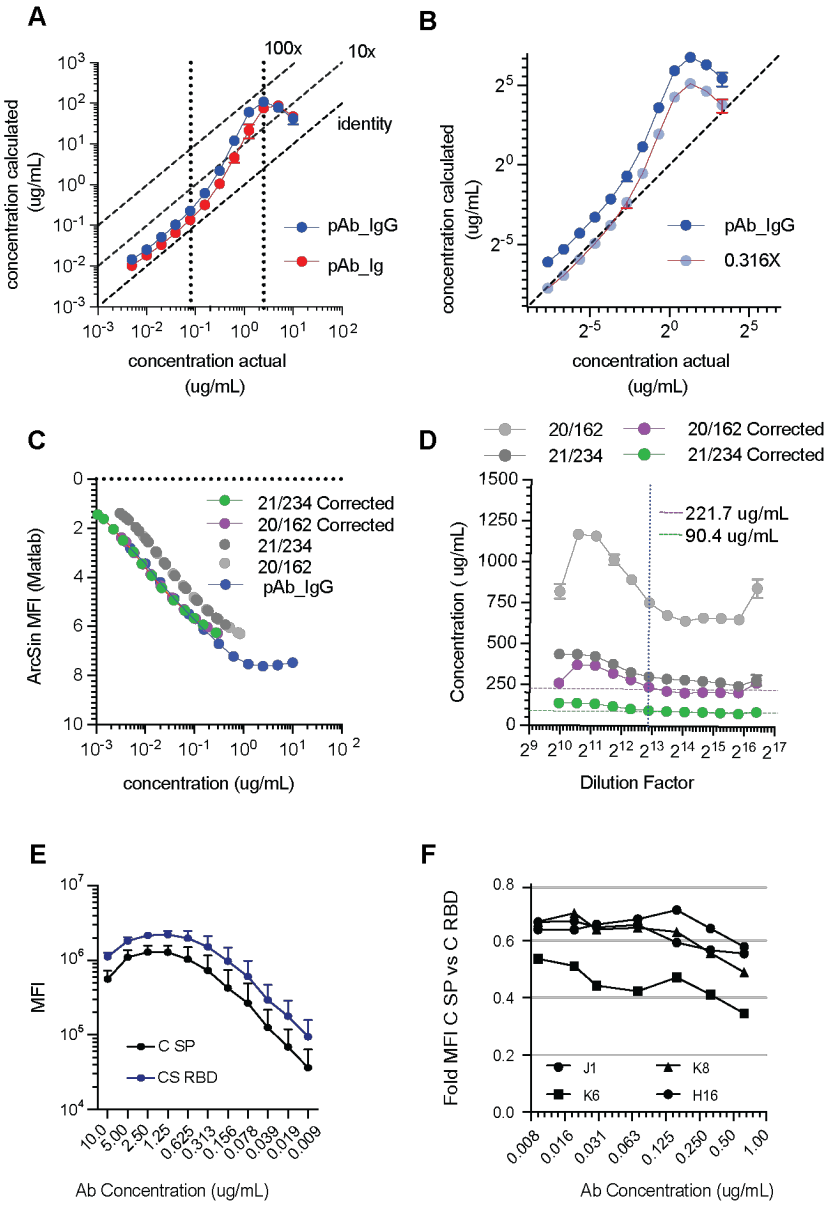

Figure 3. Quantitated subunit and polyvalency corrections. A. Extrapolated concentration of anti- CS SP pAb and pIgG plotted against the known concentration. **B**. Calculated polyvalency correction factor for anti-CS SP pAb IgG. Fold difference in MFI between CS SP and CS RBD across the linear range of dilutions is shown. **C**. ArcSIn transformed MFI values derived from the array plotted against known concentration of anti-CS SP pAb and uncorrected values derived from the indicated NISBC standards. Corrected values were generated by linear scaling of the extrapolated concentrations. **D.** Extrapolated anti-CS SP antibody concentrations (before and after polyvalent correction) of the indicated NISBC standards. Dashed lines indicated the high

confidence Ab concentration of the indicated standards. **E.** Mean MFI of the C SP coated (black) or C RBD coated (blue) beads stained the indicated concentrations of anti-CS RBD reactive rAbs. The resulting mean and SD of the MFIs of CS SP and CS RBD are shown. **F.** The ratio of the MFI of CS SP to CS RBD of the indicated anti-CS RBD rAbs at the indicated concentration.

---

well as the numbers of beads for each bead gate as shown in Figure S1. This structure array is also used to generate standard curves for each isotype, bead size and sample dilution (multiple dilutions can be run together and are annotated in the sample manifest, and each requires their own set of standard curve samples). The samples used to generate the standard curves are annotated as such in the sample manifest. These data are used to compute a four-parameter logistic (4PL) fit for each bead size/isotype/dilution as shown in Figure S2. Finally, the structure array and the 4PL fits are used to back-calculate concentration units for the MFI data, and write the entire data set as a single, tabular text file suitable for importing into any analysis program or a relational database for large-scale studies. This software is suitable for high-throughput use. In a typical configuration, data derived from five 96-well plates run on a Cytoflex (Beckman Coulter, Indianapolis IN, USA) – 480 samples including standards – can be processed in about a minute on a current model Macbook Pro with no special memory or processor requirements.

3.6 Deriving MFI Reactivity Data from a Sample

The computational workflow parallels the process for manually quantifying reactivity and is shown in Figure 4. First, MFI data are extracted from an FCS file [17] and transformed using the hyperbolic arcsine [18]. Next, a forward-scatter vs. side-scatter plot will reveal events corresponding to the different sized beads as densities of points. These are automatically detected by looking for the expected number of peaks along the forward-scatter (x) axis to define gates, and then, within each, identify single peaks on the side-scatter (y) axis. The intersection of these gates in 2-D space are used to define oval gates (Figure 4a), and events within these gates are annotated as distinct populations of

410 Figure 4.

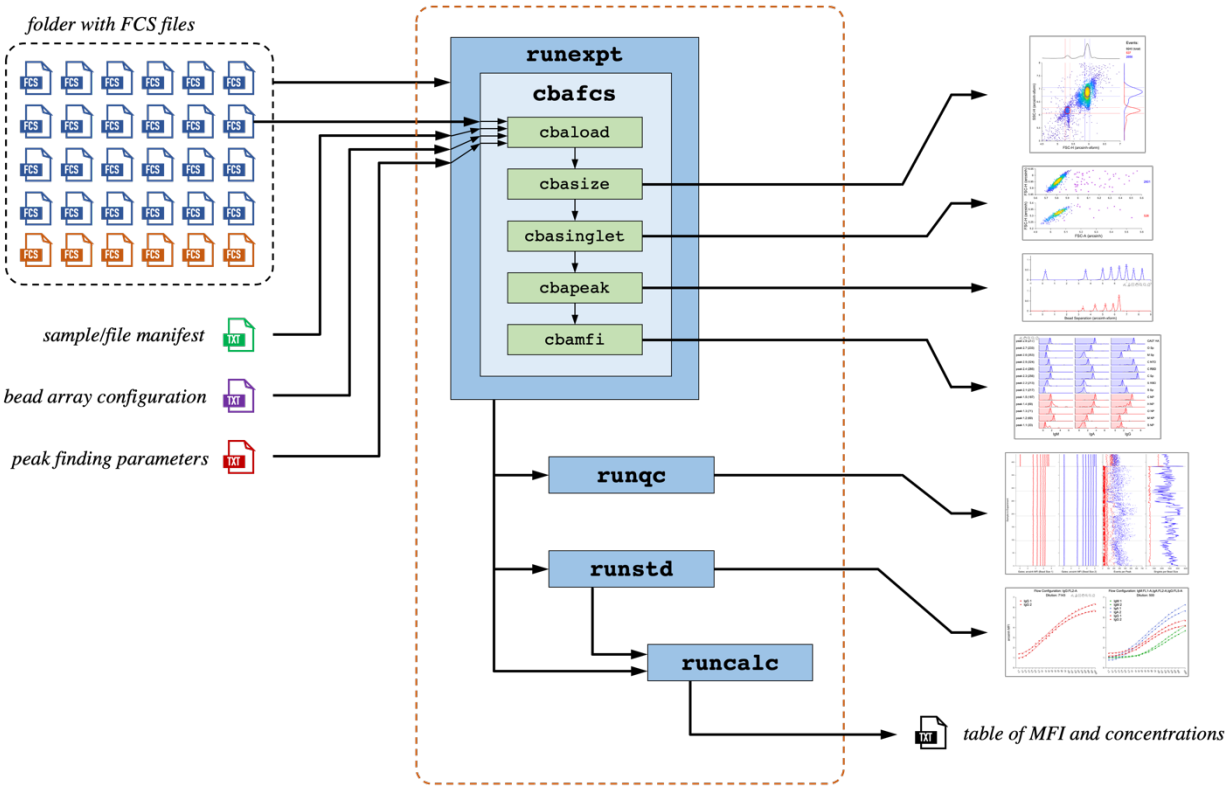

411

412 **Figure 4.** Software components are shown within red dashed box. Green boxes are
413 modules that perform a single element of processing. The light blue box is a program
414 that processes a single FCS file to extract transformed MFI data for all features in the
415 assay. The darker blue box represents a wrapper to batch process many FCS files
416 (represented in black dashed box) and annotates whether an FCS file is a normal
417 sample (blue) or a standard control sample (orange). A sample manifest is used in
418 batch mode to provide sample metadata. Additionally, a bead array configuration file
419 and a peak finding parameter file contain parameters that describe association of beads
420 with proteins and settings applied to each file. After the program is run in batch mode,
421 there are modules for bead gate quality assessment, construction of standard curves
422 and back-calculation to concentration units. When running for an individual file, figures
423 can be generated for diagnostic purposes (right).
424 beads. Next, forward-scatter height vs. area plots for events in each bead size gate are
425 evaluated using density-based clustering to identify outliers representing non-singlets that
426 are to be excluded (Fig 4b). Singlets from this step are then used for peak finding (for

each bead size gate) based on transformed MFI of the specified bead channel specified in the manifest header and compared against the expected number of peaks as indicated in the array configuration file (Fig 4c). Finally, events from each bead gate are evaluated

---

Figure 5. Raw FCS data processing steps.

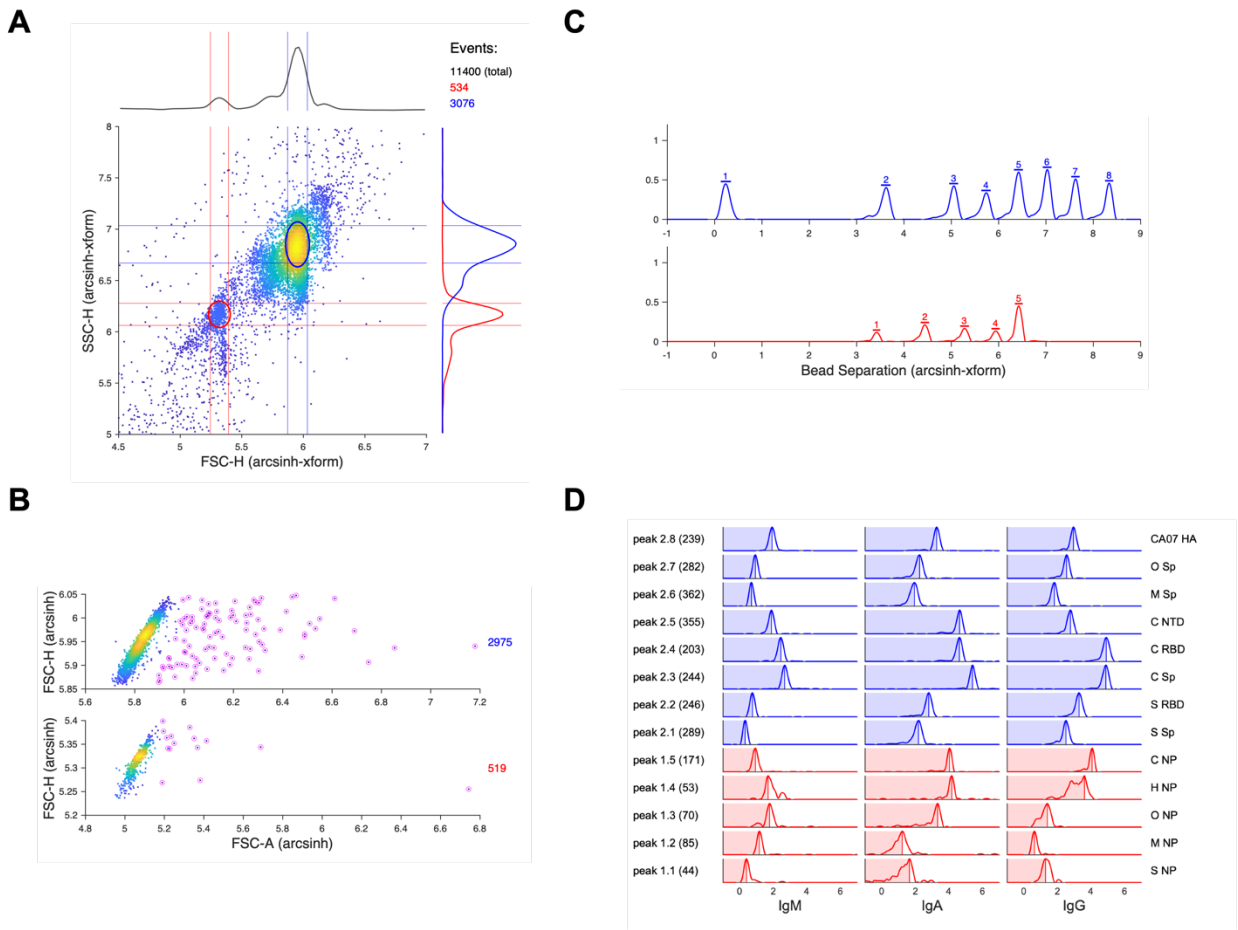

All intensity data is hyperbolic arcsin transformed. A. Forward scatter vs. side scatter to identify densities of events associated with multiple bead sizes. Red and blue ovals are gates for 4um and 5um beads, respectively. B. Density-based clustering on forward scatter height vs. area to identify outliers, or non-singlets for each bead size gate. C. Identification of peaks on the specified bead channel for each bead size after non-singlets filtered out. Line segments above each peak are individual bead gates. D. Hyperbolic arcsine MFI intensity plots on the secondary isotype channels (columns of plots) for each bead size/peak gate (rows of plots). For each row, number of beads per

gate indicated in parentheses. Antigen features for this example panel are: C = SARS-CoV-2; S = SARS-CoV-1; M = MERS; O = OC43; H = HKU-1; CA07 HA = California 07 influenza hemagglutinin; Sp = spike protein; RBD = receptor binding domain; NP = nuclear protein; NTD = n-terminal domain.

---

on the secondary isotype flow channel(s) specified in the manifest header to quantify the location of the peak (in transformed MFI) for each bead feature and isotype (Fig 4d). Details about program use and file formats can be found in the supplemental materials. Comparison of MFIs computed with the automated software to manual processing using FlowJo (BD Biosciences, Franklin Lakes NJ, USA) led to similar results, as shown in Figure S1 for four representative samples.

3.7 Polyvalency and subunit corrections:

When we began to analyze serum samples and polyclonal Ab preparations, we noted that the highest MFI values observed often eclipsed that recorded using antigen specific monoclonal Abs, suggesting that antigen-monoclonal Abs standards would result in an over extrapolation of the total antigen specific Ab in these samples, and that the cytometric array is sensitive to effects resulting from the polyvalency of Abs present in sera or other polyclonal Ab preparations. We hypothesized that multiple epitopes present on antigens were simultaneously bound resulting in higher maximum MFI values than exhibited by an equivalent concentration of a mAb, a phenomenon that would influence Ab quantification. To determine if this were the case, and to quantitate this polyvalency effect, we assayed a polyclonal C SP reactive Ab preparation derived from the serum of a vaccinated donor. Using antigen specific capture beads to quantitate the Ab isotype in this preparation, we determine it was composed of 90 percent IgG, 10 percent IgA, with low but detectable levels of IgM. Because IgA was present as a significant portion C SP reactive Ig, we further purified IgG using protein G chromatography yielding an anti-C SP pIgG with a mixture of IgG subclasses. We then evaluated both the pAb and IgG anti-C SP preparations in the CBA. As can be seen in figure 5a, the MFI of the IgG detection Abs was noticeably but marginally higher in the IgG fraction resulting from the presence

473 of IgM and IgA Abs in the Ig preparation. We then used the array to quantitate C SP Abs
474 and compared these calculated values to the known concentrations. Although the
475 calculated values were higher than the known concentrations, they exhibited a linear
476 relationship up to concentrations of approximately 0.75 ug/mL, a concentration in which
477 the prozone effects of anti-SP Abs become apparent (fig 5c). By comparing the known
478 IgG concentration with the calculated values along the serial dilutions within the linear
479 range we could determine the increase in apparent concentration resulting from the
480 polyclonality of the purified anti-C SP Ab, which was an apparent 3.16 fold inflation of the
481 calculated concentration (fig 5b). These data demonstrate the average polyvalency effect
482 within the assay is constant within the range of concentrations indicated and provided a
483 correction factor for extrapolated Ig concentration values. To further confirm this
484 normalization was accurate, we assayed the NIBSC anti-C SP standards at serial
485 dilutions ranging from 1/1e3 to 1/8.65e4. When the resulting anti-C SP values are
486 corrected and plotted against the known dilutions of the pAb anti-SP they collapse to near
487 identity, confirming the accuracy of this correction (fig 5c). Using this approach, we
488 calculate the total anti-SP IgG to be 221.7ug/mL and 90.4ug/mL in the NISBC standards
489 2-/162 and 21/324 respectively (Fig 5D).
490 In addition to the polyvalency effects described above, we noted that the MFI values
491 were higher for the CS RBD particles than for full length SP trimers. This effect was
492 manifest as exceptionally high extrapolated anti-CS RBD values in some samples.
493 Comparing the MFI of the CS RBD and C SP beads resulting from staining with dilutions
494 of four RBD reactive mAbs, we consistently observed higher values for the RBD particles
495 (fig 5e). As these Abs recognize an identical epitope on both antigens and the bead
496 constituents exhibit identical biotin binding capacity, we reasoned that because the RBD
497 is expressed as a monomer and has variable accessibility in the full-length trimers (RBD
498 up-down configurations [21]) the epitope density is unequal between these configurations.
499 To determine if this was a consistent effect, we analyzed the fold difference in MFI
500 between SP and RBD beads at a range of concentrations of four anti-RBD Abs (Fig 5f).
501 Although the CBA signal derived from mAbs is dependent on Ab affinity in addition to
502 concentration, three of these Abs exhibit a concentration independent 1.5 fold increase

in RBD MFI compared to that of

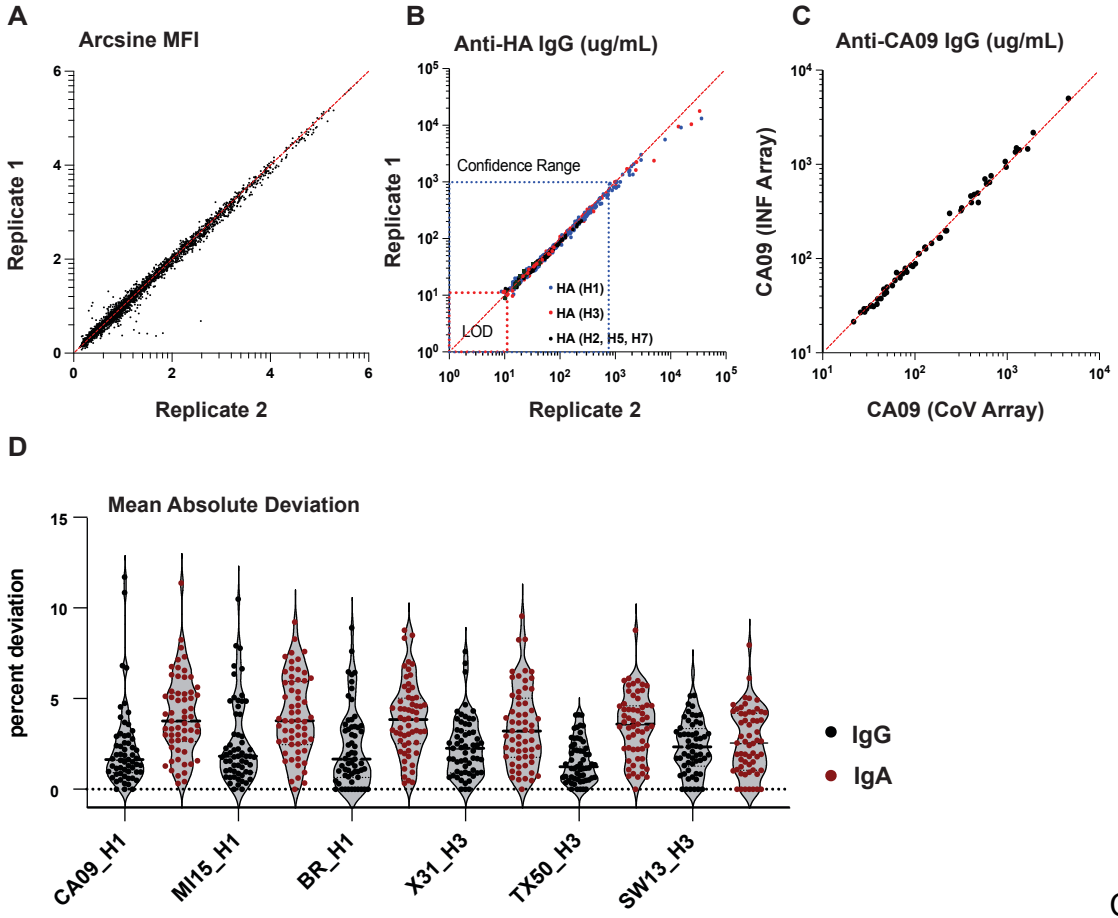

C SP

Figure 6. Reproducibility of the CBA. **A.** Scatter plot of the ArcSin MFI of each bead for all samples for two independent measurements of the CCHI U19 cohort serum. The values of the two replicates are plotted pairwise. **B**. Extrapolated antibody concentration for the two replicates ploted pairwise for the indicated HA antigens. **C**. Scatter plot of the derived concentration of Ab reactive with CA09 HA derived from the COVID and INF arrays. **D**. Mean absolute deviation for each data point of two replicates across the two replicates for the indicated antigens and Ab isotypes.

---

trimers, allowing us to correct for differences in RBD epitope availability between full length SP and monomers.

518 *3.8 Sensitivity, accuracy, and reproducibility.*

519 Although the array results are highly reproducible when assaying monoclonal antigen-
520 specific Abs or isotype specific Ab standards, we sought to determine the variance of
521 array across repeated measurements. To quantitate the reproducibility of the array
522 derived Ab values, we analyzed serum available through the UAB Comprehensive Center
523 for Human Immunology (CCHI) donor repository twice, independently, with COVID and
524 INF arrays. The MFI of each antigen in the arrays was nearly identical in the between the
525 two replicates (fig 6a). Because acquisition for most of these samples pre-dated the
526 COVID19 pandemic, they did not contain detectable SARS-CoV-2 antigen reactivity (fig
527 S3). However, IgG reactivity toward one or more HA antigens was observed in all
528 samples. The calculated value of the most prominently targeted HA antigens (including
529 both H1 and H3) were in close agreement between the replicates (fig 6b). Although
530 deviations between replicates were noted at the highest levels detected, these fall outside
531 of the linear range of the assay. Within the range of confidence, we observed a high level
532 of agreement between the two measurements. Importantly, as shown in Figure 6c, the
533 calculated values of HA CA09, which was included in the COVID array as a positive
534 control, were nearly identical in both arrays. As these reagents were generated
535 independently using different lots of SA beads, this demonstrates the reproducibility of
536 both bead generation and assay measurements. To quantitate the reproducibility of the
537 assay, we examined the mean absolute deviation of IgG and IgA reactivity toward the
538 three most frequently targeted HA H1 and H3 antigens (fig 6d). The average deviation is
539 less than 5% across all these antigens, and slightly lower for IgG (2.5%) than for IgA (4%).
540 Collectively these data suggest the arrays are highly reproducible both at the level of bead
541 generation and in their performance.

542 We did not observe Ab binding to C SP coated beads in serum samples collected
543 before the spring of 2021, despite IgG reactive with O SP being readily quantifiable in all
544 samples (serum antigen specific Ab concentrations for all antigens is shown in figure 7).
545 Following the spring of 2021, C SP reactivity was observed in 13/19 samples whereas C
546 NP reactivity was only observed in 4. In every case, C NP reactivity was corelated with C
547 SP Ab, suggestive of a prior infection (fig S3). These data are in line with the infection

548 and vaccination rates within the general population from which these donors were derived
549 [22].
550 Although HA reactivity was observed in all samples, there were significant
551 differences in the HA reactivity and Ab levels observed across individuals, representative
552 array histograms shown in Figure S4. A bias toward either H1 or H3 HA was observed in
553 some individuals, while others exhibited a balanced anti-HA Ab repertoire, although the
554 recent vaccine formulations were apparent, with CA09, Brisbane (H1) and MI15
555 demonstrated the highest level of reactivity. Reactivity toward PR8 was observed to be
556 the lowest of H1 HA (fig 7). Reactivity toward H3 were generally lower than that of H1
557 while reactivity toward the H2, H5, H7 and H9 included in the array were rarely detected.
558 Most individuals exhibited IgG and IgM Abs toward INF NP while only 10% harbored
559 serum reactivity toward INF NS1, perhaps indicative of a recent INF infection. When we
560 compared the reactivity of these antigens, we noted a significant correlation between H1
561 and H3 HA, which were poorly correlated with one another (fig 8a). Although we cannot
562 determine if this is due to cross-reactive Abs, or that similar levels of Abs that target these
563 antigens, the sequence similarity, as is the case for CA09 and MI15, are associated with
564 the highest correlation of Ab levels (fig 8bc). Interestingly, although IgG and IgA Ab levels
565 are both highly corelated toward similar HA antigens, the IgG and IgA levels themselves
566 do not correlate (fig 8c), perhaps suggestive of different origins of HA reactive Abs of
567 these isotypes. Collectively these data demonstrate the assay is suitable for high-
568 dimensional, high-throughput Ab reactivity determination.
569

570

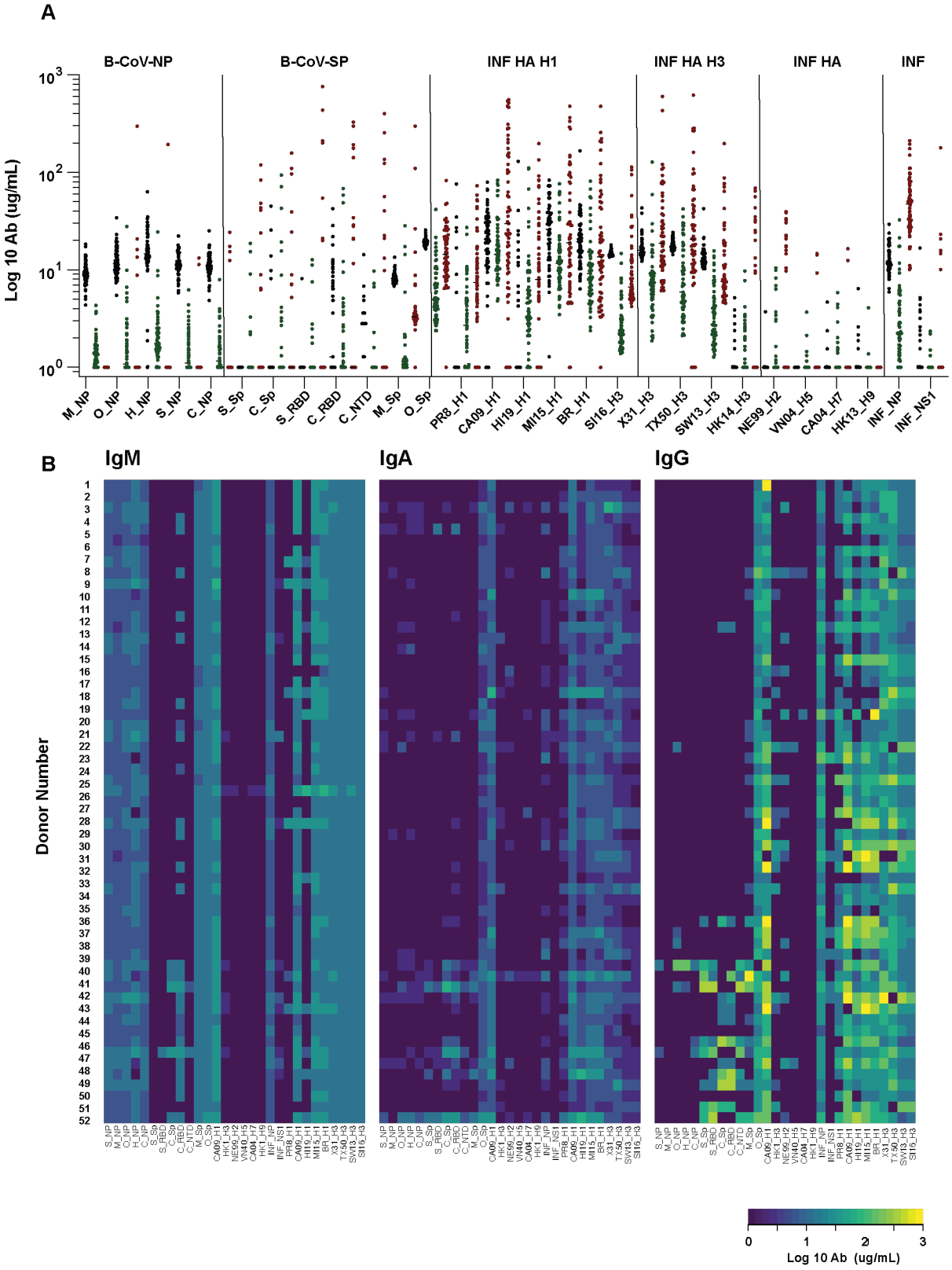
A
B-CoV-NP
B-CoV-SP
INF HA H1
INF HA H3
INF HA
INF
Log 10 Ab (ug/mL)
M_NP
O_NP
H_NP
S_NP
C_NP
S_Sp
C_Sp
S_RBD
C_RBD
C_NTD
M_Sp
O_Sp
PR8_H1
CA09_H1
HI19_H1
MI15_H1
BR_H1
SI16_H3
X31_H3
TX50_H3
SW13_H3
HK14_H3
NE99_H2
VN04_H5
CA04_H7
HK13_H9
INF_NP
INF_NS1
B
IgM
IgA
IgG
Donor Number
Log 10 Ab (ug/mL)

571 **Figure 7.** The reactivity profiles of 96 sera samples toward the full BCov and INF
572 arrays. **A.** The concentration of IgM, IgA, and IgG reactive with the indicated antigen as
573 measured by the Coba and INF array. **B.** Heatmap of the log10 Ab concentration
574 (ug/mL) for the indicated antigen. Each row corresponds to an individual serum, and
575 each column corresponds to the indicated antigen, IgM, IgA, and IgG are shown.

576

577

578 4. Conclusions

579 Here we describe an CBA platform designed to conduct high-throughput determination of
580 Abs reactive with viral antigens. The assay provides a rich view of the humoral immune
581 landscape by multiplexing the analysis of 12 B-CoV or 16 INF antigens into a single
582 assays. By altering dilutions factors and secondary detection reagents, the levels of IgG,
583 IgM, and IgA can be accurate determined. This platform exhibits high sensitivity, although
584 the lower limit of detection is dependent on dilution factor, as little as 2ng/mL of antigen-
585 specific IgG in the final dilution can be measured. The assay demonstrates high
586 specificity, as demonstrated by multiple monoclonal Abs, the reactivity to each antigen in
587 the array is discrete. The use of multiple indirect standards provides accurate
588 quantification for Ab reactive to each antigen across all assayed isotypes. Additionally,
589 the assay requires minute amounts of both antigen and serum tested, typically consuming
590 less than 0.5ug of antigen and less than 1uL of sample per assay.

591 Although, the CBA array described here is focused on B-CoV and INF serology, the same
592 strategy can be implemented to evaluate serum Ab to a wide array of antigenic targets.

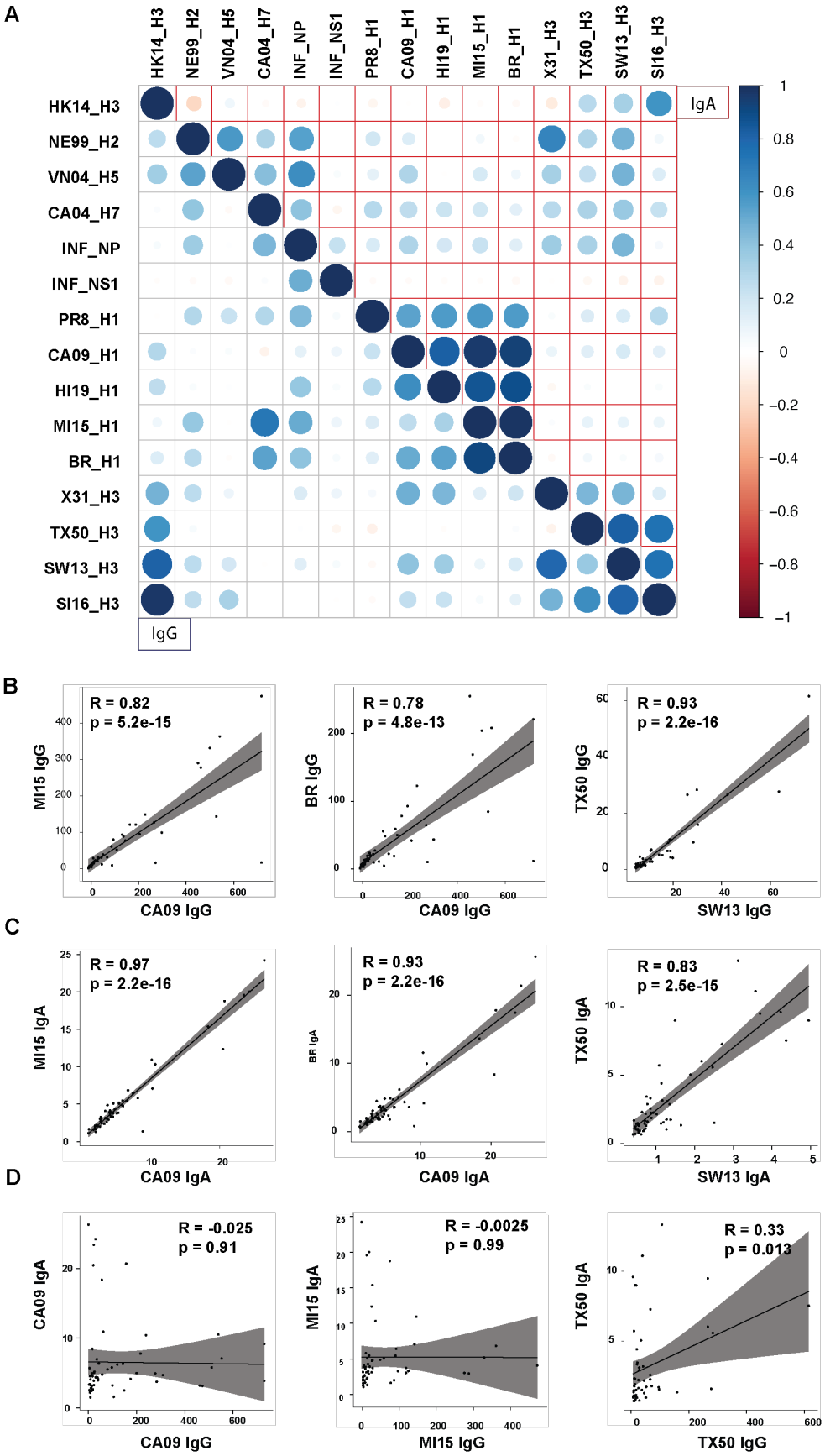
A
HK14_H3
NE99_H2
VN04_H5
CA04_H7
INF_NP
INF_NS1
PR8_H1
CA09_H1
HI19_H1
MI15_H1
BR_H1
X31_H3
TX50_H3
SW13_H3
SI16_H3
IgA
IgG
1
0.8
0.6
0.4
0.2
0
−0.2
−0.4
−0.6
−0.8
−1
B
R = 0.82
p = 5.2e-15
MI15 IgG
CA09 IgG
R = 0.78
p = 4.8e-13
BR IgG
CA09 IgG
R = 0.93
p = 2.2e-16
TX50 IgG
SW13 IgG
C
R = 0.97
p = 2.2e-16
MI15 IgA
CA09 IgA
R = 0.93
p = 2.2e-16
BR IgA
CA09 IgA
R = 0.83
p = 2.5e-15
TX50 IgA
SW13 IgA
D
R = -0.025
p = 0.91
CA09 IgA
CA09 IgG
R = -0.0025
p = 0.99
MI15 IgA
MI15 IgG
R = 0.33
p = 0.013
TX50 IgA
TX50 IgG

593

Figure 8. Correlation of Ab levels for HA antigens in the array**. A.** The pairwise Pearson correlation coefficient for either IgG (lower left) or IgA (upper right) of Ab levels for each antigen in the INF Array. **B.** Scatter profiles of antibody levels toward the indicated H1 and H3 hemagglutinins for the 59 samples in the cohort.

The use of recombinant antigens, like the various SP ectodomains and subunits or HA and NP described here, allow for the rapid replacement or addition of similar antigens into the CBA with no required modification to the analytics. Although the corrections for polyvalency and subunit epitope availability are specific for C SP, these are the product of the physical nature of the antigens included in the current array, and whether such corrections are applicable to other antigens necessitates empirical determination. Polyclonal corrections may be generalizable, however, as the number of individual Abs that may simultaneously bind their cognate antigen is influenced by immunodominance of epitopes and steric hindrance, an idea supported by structural studies [23-25].

The high-dimensional assay we described greatly benefits from the use of the automated analytic platform. When combined, this system facilitates the rapid and accurate determination of antigen reactive Ab. Although the source material used as examples in this study are serum, the assay is amenable to many biological samples including nasal washes and saliva. The capacity to visualize both the magnitude and breadth of Ab responses to vaccination or infection with respiratory pathogens is valuable in determining correlates of protection derived from vaccination or pathogen exposure, and the ability to easily and rapidly expand the antigens incorporated into the array with minimal effects on the established analytics makes this approach an attractive option to fill the continuing need for large-scale serology studies.

619

620 1. Garcia-Beltran, W.F., et al., *Multiple SARS-CoV-2 variants escape neutralization by*
621 *vaccine-induced humoral immunity.* Cell, 2021. **184**(9): p. 2372-2383 e9.
622 2. Yadav, P.D. and S. Kumar, *Global emergence of SARS-CoV-2 variants: new foresight*
623 *needed for improved vaccine efficacy.* Lancet Infect Dis, 2022. **22**(3): p. 298-299.
624 3. Meyer, B., C. Drosten, and M.A. Muller, *Serological assays for emerging coronaviruses:*
625 *challenges and pitfalls.* Virus Res, 2014. **194**: p. 175-83.
626 4. Pisanic, N., et al., *COVID-19 Serology at Population Scale: SARS-CoV-2-Specific Antibody*
627 *Responses in Saliva.* J Clin Microbiol, 2020. **59**(1).
628 5. Caceres-Martell, Y., et al., *Single-reaction multi-antigen serological test for comprehensive*
629 *evaluation of SARS-CoV-2 patients by flow cytometry.* Eur J Immunol, 2021. **51**(11): p.
630 2633-2640.
631 6. Cameron, A., et al., *A Multiplex Microsphere IgG Assay for SARS-CoV-2 Using ACE2-*
632 *Mediated Inhibition as a Surrogate for Neutralization.* J Clin Microbiol, 2021. **59**(2).
633 7. Dawson, E.D., et al., *Multiplexed, microscale, microarray-based serological assay for*
634 *antibodies against all human-relevant coronaviruses.* J Virol Methods, 2021. **291**: p.
635 114111.
636 8. Egia-Mendikute, L., et al., *Sensitive detection of SARS-CoV-2 seroconversion by flow*
637 *cytometry reveals the presence of nucleoprotein-reactive antibodies in unexposed*
638 *individuals.* Commun Biol, 2021. **4**(1): p. 486.
639 9. Guarino, C., et al., *Development of a quantitative COVID-19 multiplex assay and its use for*
640 *serological surveillance in a low SARS-CoV-2 incidence community.* PLoS One, 2022. **17**(1):
641 p. e0262868.
642 10. Jolley, M.E., et al., *Particle concentration fluorescence immunoassay (PCFIA): a new, rapid*
643 *immunoassay technique with high sensitivity.* J Immunol Methods, 1984. **67**(1): p. 21-35.
644 11. Kenny, G., et al., *Performance and validation of an adaptable multiplex assay for detection*
645 *of serologic response to SARS-CoV-2 infection or vaccination.* J Immunol Methods, 2022:
646 p. 113345.
647 12. Roy, D.R., et al., *Development, Validation, and Utilization of a Luminex-Based SARS-CoV-*
648 *2 Multiplex Serology Assay.* Microbiol Spectr, 2023: p. e0389822.
649 13. Morgan, E., et al., *Cytometric bead array: a multiplexed assay platform with applications*
650 *in various areas of biology.* Clin Immunol, 2004. **110**(3): p. 252-66.
651 14. Allie, S.R., et al., *The establishment of resident memory B cells in the lung requires local*
652 *antigen encounter.* Nat Immunol, 2019. **20**(1): p. 97-108.
653 15. Beckett, D., E. Kovaleva, and P.J. Schatz, *A minimal peptide substrate in biotin holoenzyme*
654 *synthetase-catalyzed biotinylation.* Protein Sci, 1999. **8**(4): p. 921-9.
655 16. Nellore, A., et al., *A transcriptionally distinct subset of influenza-specific effector memory*
656 *B cells predicts long-lived antibody responses to vaccination in humans.* Immunity, 2023.
657 17. fca, B.L. *readfcs.m* balkay.laszlo@med.unideb.hu, Department of Medical Imaging,
658 University of Debrecen. Version 22/Jun/2020. Matlab File Exchange. 2020; Available from:
659 https://www.mathworks.com/matlabcentral/fileexchange/9608-fca_readfcs.
660 18. Finak, G., et al., *Optimizing transformations for automated, high throughput analysis of*
661 *flow cytometry data.* Bmc Bioinformatics, 2010. **11**.

662 19. G., C. *L4P.m, Four parameters logistic regression - There and back again (2012)*. Matlab
663 File Exchange. 2012; Available from:
664 https://it.mathworks.com/matlabcentral/fileexchange/38122.
665 20. R., H. *Flow Cytometry Data Reader and Visualization* 2021; Available from:
666 https://www.mathworks.com/matlabcentral/fileexchange/8430-flow-cytometry-data-
667 reader-and-visualization.
668 21. Henderson, R., et al., *Controlling the SARS-CoV-2 spike glycoprotein conformation.* Nat
669 Struct Mol Biol, 2020. **27**(10): p. 925-933.
670 22. Health, A.D.o.P. *Coronavirus Disease 2019 (COVID-19)*. 2023; Available from:
671 https://www.alabamapublichealth.gov/covid19/.
672 23. Barnes, C.O., et al., *Structures of Human Antibodies Bound to SARS-CoV-2 Spike Reveal*
673 *Common Epitopes and Recurrent Features of Antibodies.* Cell, 2020. **182**(4): p. 828-842
674 e16.
675 24. Nogal, B., et al., *Mapping Polyclonal Antibody Responses in Non-human Primates*
676 *Vaccinated with HIV Env Trimer Subunit Vaccines.* Cell Rep, 2020. **30**(11): p. 3755-3765
677 e7.
678 25. Han, J., et al., *Polyclonal epitope mapping reveals temporal dynamics and diversity of*
679 *human antibody responses to H5N1 vaccination.* Cell Rep, 2021. **34**(4): p. 108682.
680